

Informing Urban Flood Risk Adaptation by Integrating Human Mobility Big Data During Heavy Precipitation

Published as part of Environmental Science & Technology virtual special issue "Accelerating Environmental Research to Achieve Sustainable Development Goals."

Jiacong Cai, Jianxun Yang*, Miaomiao Liu*, Wen Fang, Zongwei Ma, and Jun Bi



Cite This: *Environ. Sci. Technol.* 2024, 58, 4617–4626



Read Online

ACCESS |

Metrics & More

Article Recommendations

Supporting Information

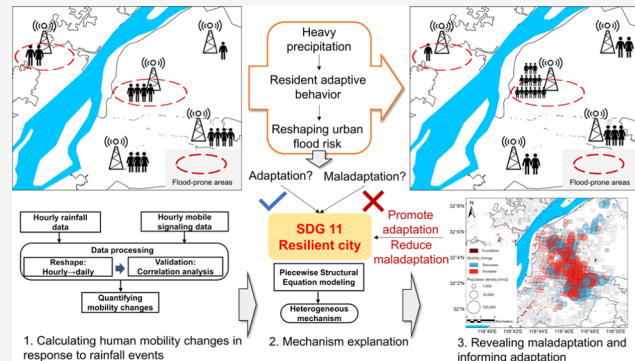
ABSTRACT: Understanding the impact of heavy precipitation on human mobility is critical for finer-scale urban flood risk assessment and achieving sustainable development goals #11 to build resilient and safe cities. Using ~2.6 million mobile phone signal data collected during the summer of 2018 in Jiangsu, China, this study proposes a novel framework to assess human mobility changes during rainfall events at a high spatial granularity (500 m grid cell). The fine-scale mobility map identifies spatial hotspots with abnormal clustering or reduced human activities. When aggregating to the prefecture-city level, results show that human mobility changes range between -3.6 and 8.9%, revealing varied intracity movement across cities. Piecewise structural equation modeling analysis further suggests that city size, transport system, and crowding level directly affect mobility responses, whereas economic conditions influence mobility through multiple indirect pathways. When overlaying a historical urban flood map, we find such human mobility changes help 23 cities reduce 2.6% flood risks covering 0.45 million people but increase a mean of 1.64% flood risks in 12 cities covering 0.21 million people. The findings help deepen our understanding of the mobility pattern of urban dwellers after heavy precipitation events and foster urban adaptation by supporting more efficient small-scale hazard management.

KEYWORDS: urban flood risk, human mobility, mobile phone big data, adaptation, small-scale hazard

1. INTRODUCTION

Cities around the globe have witnessed a growing number of flooding events and their catastrophic impacts in the past few decades.^{1,2} Urban flood inundation happens when rainfall overwhelms the capacity of the drainage system.³ Floods result in drastic damage to urban infrastructure including the water supply system, energy transmission and distribution facilities, and the transport system.⁴ Between 1980 and 2013, the global direct economic losses due to floods exceeded \$1 trillion and 220 000 people lost their lives.⁵ It is estimated that average global flood losses will increase to over \$60 billion per year in 2050 under projected socioeconomic and climate change pathways.⁶ Without adaptive strategies, the frequency and intensity of urban floods are expected to continuously increase.^{7–9}

Sustainable development goal (SDG) #11 (building sustainable cities and communities), introduced in 2015 alongside the other 16 goals by the United Nations, is grounded in addressing critical global issues.¹⁰ These goals serve as a collective blueprint for promoting peace and prosperity for people and the planet, both presently and in the



future.¹¹ SDG #11 focuses on creating cities and human settlements that are inclusive, safe, resilient, and sustainable. This goal places substantial emphasis on improving the resilience of cities to natural and climate change-induced disasters.¹² Effective adaptation strategies are urgently needed to manage urban floods and buffer their impacts, thereby advancing the objectives of SDG #11.^{13,14}

Various interventions can be explored for urban flood adaptation, such as waterproof infrastructure, early warning systems, nature-based solutions, and risk financing schemes. Fine-scale mapping of flood risk is a fundamental prerequisite for performing all these adaptive measures in a targeted way.^{15,16} It helps identify hotspots and drivers of inundation and supports high-efficiency resource allocation. Previous

Received: April 27, 2023

Revised: February 15, 2024

Accepted: February 16, 2024

Published: February 29, 2024



studies have proposed indicator frameworks to map urban flood risks, measured as the product of flood hazard, vulnerability, and exposure.^{17,18} Despite these efforts, data availability is always an obstacle for further applying index-based approaches at finer spatial scales.¹⁹ Moreover, setting indices and weights is a subjective process. Existing studies focus heavily on infrastructural and socioeconomic factors that may affect vulnerability. Influencing factors of exposure are often overlooked, failing to reflect the situation in the real world. Human mobility, for example, a variable that shapes dynamic urban flood exposure of residents, has not been comprehensively examined in existing flood risk mapping frameworks.^{20,21}

Urban human mobility reflects the interaction process between individuals and physical settings in the city, offering a new perspective on urban flood risk mapping and adaptation.^{22,23} Heavy rain events alter human activity patterns. When rainfall hits, urban residents may change their routine, shift to more usage of public transport, seek shelters and take refuge in concrete buildings, cancel their trips, or just stay in their cars due to road closures.²⁰ Such spontaneous intracity movement, and consequently uneven population distribution, may reshape the spatial patterns of flooding exposure within the urban area. When a large number of people gather in risk-prone places such as low buildings and crowded roads, the proportion of the population exposed to floods can potentially increase as a result.²⁴ Therefore, tracking human mobility when heavy rainfall and flood events occur is critical to understanding dynamic mappings of urban flood risks.

Current index-based assessment frameworks make it difficult to measure the effect of human mobility in response to heavy rainfall on urban flood risks. Most studies chose proxy variables to represent a city's capacity to tolerate flooding and maintain large-volume population mobility, such as access to public transport infrastructure, road densities, or percent population owing vehicles.^{25,26} These measures do not capture trajectories of urban population during extreme weather events and reflect an overall status over a long period. To identify flood risk hotspots induced by intracity population movement, it is necessary to trace human mobility patterns during the time span of heavy precipitation events.

In recent years, increasing accessibility to real-time geolocated big data, such as mobile phone records, check-ins of online social media, and GPS traces of vehicles, has enabled researchers to model human mobility patterns at an unprecedented spatial and temporal resolution.^{27,28} Utilizing massive human trajectory data emerges as a research frontier in the field of disaster risk management.²⁹ These data sets are powerful to track and explain human behaviors after emergent events or disasters. For instance, geolocated big data have been employed to monitor migration, recovery of small businesses, and public emotional responses after natural hazards.^{30,31} Regarding the effect of heavy precipitations and urban floods on the citizens' mobility, several studies attempted to quantify the magnitude of impacts or the ability to recover from the perturbation.³² Preliminary conclusions drawn from these studies suggest that rainfalls may have a reducing effect on the citizen's trip flows, distance, and duration. However, very few of them take a step further to estimate how human mobility leads to highly heterogeneous population distribution and, consequently, results in dynamic urban flood risk exposure. Another major gap in the literature is that these studies mostly

focus on a single city or a few case cities, which makes it hard to explain variations across cities and recommend practical and effective adaptive interventions for other regions.^{33,34}

To close the research gaps in urban flood risk mapping and inform adaptation at finer scales, this study developed a novel detrending framework and pictured rainfall-induced mobility perturbation at a high spatial resolution (500 m grid cell), leveraging a data set of ~2.6 million mobile phone records obtained during 2018 summer in Jiangsu Province, China. Emerging hot–cold spots of mobility variation were identified, revealing the shocks in citizens' daily routines facing heavy precipitation events. We then aggregated grid estimates on the urban scale and employed piecewise SEM to elucidate the variations in population mobility changes across cities. Finally, we superimposed a historical flood inundation map onto the mobility map to reveal how mobility changes reshape urban flood risk exposure. It is anticipated that our findings will help decision-makers better understand the mobility pattern of urban citizens impacted by heavy rainfall events, which can support more efficient adaptation resource allocation and accelerate progress in achieving SDGs #11.

2. LITERATURE REVIEW

Geolocated big data have radically changed the ways through which human societies manage natural disasters due to their varied possibilities in pattern mining and trend prediction. To track advances in related fields and disclose research gaps, we briefly review the applications of geolocated big data (especially mobile phone data) in tracking human mobility and improving natural hazard adaptation.^{30–32}

Geolocated big data are often user-generated and provide precise location information on individual users. These extensive data sets are primarily sourced from personal mobile devices, including social media posts, call detail records, and web search queries. Among all types of geolocated data sets, mobile phone location data are advantageous in their rapid and high-frequency data collection, stable longitudinal time frame, and wide population coverage. This stability in data collection ensures that mobile phone signals can predict human mobility with remarkable accuracy even in chaotic situations, reaching levels as high as 95%.^{35,36} This feature enables researchers to observe, estimate, and model human digital geographical footprints at unprecedented granularity. We emphasize three pivotal areas in which mobile phone data can deepen our knowledge of human mobility and hazard adaptation.

2.1. Tracking Mobility Response After Small-Scale Shocks. Most geolocated data sets, without enough temporal density and stable monitoring of individual users (e.g., social media posts), have focused on mobility tracking after unique large-scale disasters. However, some small-scale events, such as traffic jams, crowding, and also rainfall anomalies involved in this study, may only cause short-term mobility variations in small-scale regions but may lead to intensive exposure to risks. In this case, mobile phone signal data are more capable of capturing the dynamics due to their higher spatial–temporal granularity. For example, Perazzini et al.³⁷ leveraged mobile phone data to estimate people crowding and traffic intensity in small urban areas, which can help effectively mitigate exposure to natural disasters while ensuring the quality of life at the “small area” level.

2.2. Monitoring Natural or Human-Made Intervention Effects. Another important feature of mobile phone position data is that they are collected automatically and at

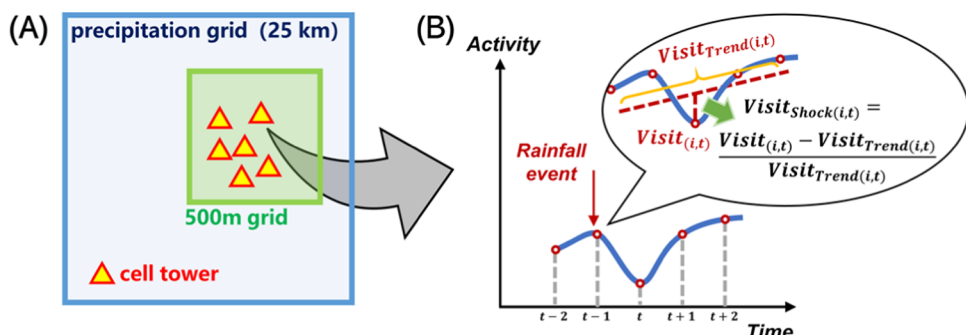


Figure 1. Data processing steps that calculate grid-level mobility changes after heavy rainfalls. (A) Spatial overlay of cell tower, 500 m fishnet grid, and 25 km precipitation grid. (B) Conceptualization of the process to calculate tower-level visit changes due to the shock of rainfall events.

high frequency, which ensures a stable, continuous, and adequate number of data samples. Therefore, they are useful for evaluating the intervention effects of both natural events and external human manipulations. For example, Qian et al.³² examined rainstorms and geotagged behaviors (measured by smartphone location data) in eight cities. They found city residents' mobility anomalies disrupted by rainstorms are significant, and the sensitivity varies in different cities. Mobile phone data are also used to examine the controlling effect of mobility restriction during the recent coronavirus (COVID-19) pandemic. Lai et al.³⁸ analyzed anonymous mobile phones in Shenzhen, China, and showed that various types and magnitudes of lockdowns are effective in curbing COVID-19 outbreaks.

3.3. Explaining Influencing Factors of Human Mobility. Understanding why people change mobility patterns is crucial in predicting individual mobility trajectories and making interventions at an early stage.^{36,39} Since mobile phone data provide continuous observation of individual user's specific behavior, it serves as a link to understand mobility decision-making in real time.⁴⁰ For example, González et al.⁴¹ analyzed the trajectory of 100 000 anonymized mobile phone users and found that human trajectories show a high degree of temporal and spatial regularity. Buckee et al.⁴² discussed the potential of using mobile phone data as useful proxies for behavioral drivers of disease transmission and investigated social, economic, and cultural forces to shape patterns of exposure. Leveraging these advantages of mobile phone big data, in this study, we attempt to address research existing gaps in urban flood risk mapping by quantifying human mobility changes triggered by small-scale natural intervention events (i.e., heavy precipitation), explaining driving factors across cities, and informing urban flood risk adaptation.

3. METHODS AND MATERIALS

3.1. Mapping Changes in Human Mobility Patterns After Heavy Rainfalls. **3.1.1. Study Region.** Located on the eastern coast of China, Jiangsu stands out as one of the highly developed provinces (see the location and population in Figure S1). By the year 2020, Jiangsu province had achieved a remarkable gross domestic product (GDP) of around 1.6 trillion USD, placing it on par with significant global economies, such as Canada, Russia, and South Korea. Notwithstanding its elevated level of development, Jiangsu is exposed to significant risks attributed to its low elevation and comparatively high annual average rainfall, typically ranging from 800 to 1200 mm.⁴³ The distinctive geographical and

climatic attributes position Jiangsu Province as the optimal choice for our primary research focus.

3.1.2. Mobile Phone Signaling Data Collection and Preprocessing. We obtained anonymized mobile phone cellular signaling data from China Telecom, one of the largest telecommunication companies in China. The research design and the use of human-related signaling data involving privacy issues have gained ethical approval from the Research Committee of the School of Environment, Nanjing University (NO. NJUSE20230613). China Telecom owns ~28 million mobile phone users in Jiangsu, accounting for ~35% of its total population.⁴⁴ The anonymized data set included 2.6 million records from 90 000 mobile phone towers in Jiangsu and covered the period from June 1, 2018, to September 30, 2018 (see example data in Table S1, locations of towers in Figure S4), during which time the middle and lower reaches of the Yangtze River in China had already entered the monsoon season and were hit by urban flooding due to excessively rainfall.⁴⁵

Each mobile phone tower recorded user requests, including calls, messages, Internet access, and other mobile phone uses per hour per day. If a person makes multiple accesses to the same tower within 1 h, it is recorded as a single visit. Figure S2 showed that daily visits had a significant ($R = 0.69, p < 0.001$) correlation with the grid population, demonstrating that our data set had a good representation of the local population and human mobility patterns.

We then aggregated the signal data from hourly to daily excluding the time window from 0:00 am to 6:00 am, as it had been pointed out in the literature that nighttime rains had no significant impact on human activities.³² To remove the effect of short-term weekly fluctuations as well as the long-term increasing trend of mobile phone users, we further applied the Seasonal Hybrid Extreme Studentized Deviate algorithm to remove these trend components.⁴⁶ More details of this method can be found in the Text S1.

3.1.3. Identifying Heavy Rainfall Events. To identify rainfall events, we first obtained hourly simulated precipitation data derived from the European Centre for Medium-Range Weather Forecasting with a spatial resolution of 0.25° (~25 km).⁴⁷ The grid-level simulated precipitation data were validated against the monitoring station data set, which showed a high correlation ($R = 0.82, p < 0.001$) (Figure S3(A)). We then simply aggregated the hourly rainfall data to daily and only kept heavy rainfall events with accumulated 24 h rainfall of more than 25 mm, according to the standards set by the China Meteorological Administration.⁴⁸ In the end, we

recognized a total of 1082 rainfall events in 37 days. Figure S3 presents the frequency of rainfall events.

3.1.4. Quantifying Changes in Human Mobility at the 500 m × 500 m Grid Level. Mobile phone towers are typically hundreds of meters apart in urban areas.⁴⁹ To this end, we developed a framework to quantify changes in human mobility patterns for each mobile phone tower. The process was schematically presented in Figure 1.

We first assigned each tower to a precipitation grid (25 km) based on its geo-coordinates. Then, for a specific rainfall event, we calculated a five-day moving average visit for each cell tower to reflect an average activity trend without the shock of rainfall, as shown in eq 1,

$$\text{visit}_{\text{trend}(i,t)} = \frac{\sum_{t-2}^{t+2} \text{visit}_{(i,t)}}{5} \quad (1)$$

Specifically, $\text{visit}_{(i,t)}$ is the number of visits recorded by tower i on rainy day t . We assumed that human activity near a cell phone signal tower will keep a linear trend as time goes by without disturbance of the rainfall event, as shown in Figure 1(B). Hence, $\text{visit}_{\text{trend}(i,t)}$, which calculates the mean tower visits in five consecutive days (including 2 days before and 2 days after the rainfall event), can serve as a baseline in the absence of heavy rain. We also performed sensitivity analysis by using 3- and 7-day moving averages as the calculation baseline and removing multiday consecutive rainfall events. The results, as reported in Figure S7, indicate that the 5-day moving average derives the most robust result. At the same time, we also compared whether the data on the rainy day should be included in the calculation of the baseline; see Texts S2 and S4 for details.

Next, to show the impact of specific rainfall events on human activity, we used eq 2 to get $\text{visit}_{\text{shock}(i,t)}$, the percentage changes between the baseline visits and the rainy day visits of tower i .

$$\text{visit}_{\text{shock}(i,t)} = \frac{\text{visit}_{(i,t)} - \text{visit}_{\text{trend}(i,t)}}{\text{visit}_{\text{trend}(i,t)}} \times 100\% \quad (2)$$

Also, it is worth noting that each cell tower might experience several precipitation events in the time span of our research. We simply calculated the average change in visits for each tower, as shown in eq 3, where N is the total number of rainfall events that have occurred covering tower i . This indicator, on the other hand, can reflect the overall perturbations of human mobility in the surrounding area when rainfall events occur. Large variations in cell phone tower visits indicated that the region is more sensitive to the impact of local rainfall events.

$$\text{visit}_{\text{shock}(i)} = \frac{\sum \text{visit}_{\text{shock}(i,t)}}{N} \quad (3)$$

Finally, in order to compile a mobility map for the whole province at a high spatial resolution, we manually created a 500 m × 500 m grid layer and joined each tower to a corresponding grid cell. We chose this spatial resolution because the radius of the tower signal coverage is about 500 m.⁴⁹ Also, a grid cell might contain multiple towers in a populous urban area. We therefore directly calculated the mean tower-level visit shocks in each grid cell to measure human mobility responses to heavy rainfall events at the 500 m × 500 m grid level. This high-resolution map could help identify hotspots of changes in human mobility within the city.

3.2. Explaining Prefecture-Level Variations in Human Mobility Change.

After mapping human activity variations after rainfall events, we attempted to reveal key factors that drive different levels of mobility change across cities. It is not feasible to explain mobility changes at the grid cell level due to the lack of information at such high resolution and the risk of model overfitting because of the large samples. Therefore, we aggregated grid human mobility changes to the prefecture level according to urban administrative boundaries,⁵⁰ trying to identify influencing factors at the city level. It should be noted that mobility changes in a city may not be balanced, so positive aggregated values may indicate abnormal crowding and minus aggregated values indicate overall reduced activity. Considering that sparsely populated grid cells might disproportionately contribute to our observations, we used the grid population as a weight in the aggregation process. A total of 53 urban areas in Jiangsu province were included here to build up models and explain factors that may determine the difference in mobility changes across cities. Detailed city location, administrative boundary, and background information were presented in Figure S4 and Table S2.

Our primary goal is to elucidate the heterogeneity in human mobility across cities. In order to scrutinize and model the intricate relationships among multiple variables concurrently, we employed the piecewise SEM to assess the connections between indicators (see the rationale for selecting piecewise SEM in Text S3). The use of piecewise SEM enables the breakdown of the overall path into a sequence of structured equations. This transition from global to local estimation provides flexibility for fitting diverse distributions and adapting to various sampling designs.⁵¹ Moreover, from a theoretical standpoint, it facilitates the fitting of smaller data sets, aligning well with the specific conditions of this study.⁵² We focused on four latent variables, namely, “city size,” “transportation,” “crowding,” and “economy.” The conceptual model is reported with the result in Figure 3.

Specifically, the first latent variable “city size” measures the level of urban development including two observational variables, i.e., built-up land area and total population. It is assumed that larger urban size and population involve more complex human movement, predict abnormal crowding, and thus increase mobility. The second latent variable “transportation” directly influences the mobility of local residents during emergencies. It is anticipated that a city with well-developed transport systems can offer more alternative traveling options when heavy rainfall occurs and thus can reduce mobility and avoid risks. Here, we select two observational variables to reflect urban transport, including bus stop density and vehicles per capita. The third latent variable, so-called “crowding”, measures social factors that may induce abnormal behaviors. We included two observational variables, i.e., population density and ratio of vulnerable populations (e.g., the old). Regions with a high population density and elderly people with limited mobility may increase the likelihood of accidental crowding. The last latent variable “economy” reflects a city’s economic condition. Developed cities may have more robust infrastructure to reduce mobility and avoid overwhelming shocks or have a large density of buildings like food courts, shopping malls, and entertainment centers that may cause crowding.⁵³ We considered two observational variables, including total GDP and per capita GDP. Finally, we introduced latent variables “mobility” (urban average mobility changes) to explore more potential pathways.

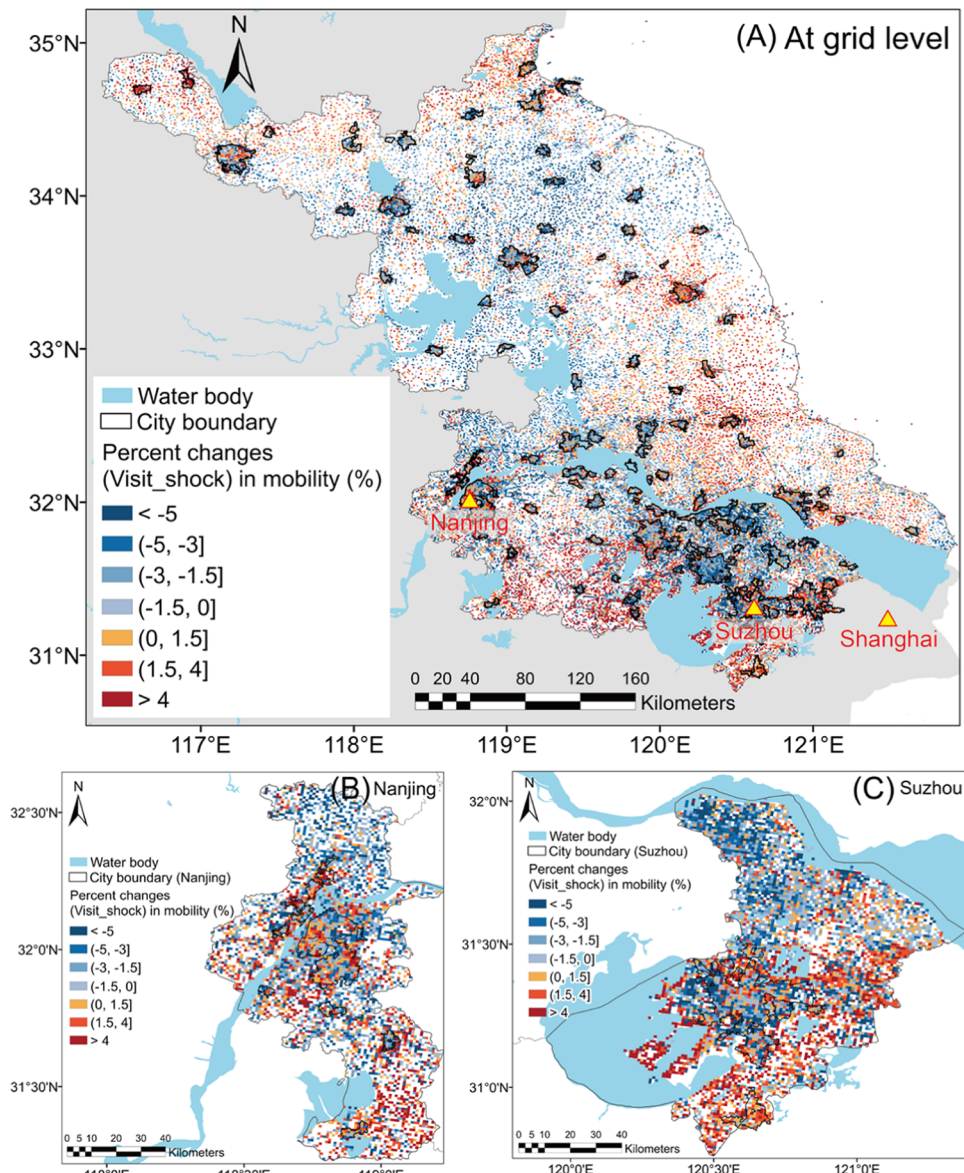


Figure 2. Mapping human mobility changes in response to rainfall events. (A) Changes in human mobility (i.e., indicator $\text{visit}_{\text{shock}}$) after rainfall at the grid level (500 m). Urban boundaries with dense populations are marked by bold solid lines. (B, C) Enlarged view of Nanjing and Suzhou urban agglomeration areas.

Due to length limits, we report conceptual model and coefficient estimates together in the results and report data sources of observational variables and modeling details in the Supporting Information (Tables S3 and S4).

3.3. Calculating Mobility-Induced Variations in Urban Flood Risk Exposure. Changing mobility patterns can be regarded as an individual adaptation to rainfall because people may change their routines to avoid urban inundation or traffic. However, it is questionable whether these behaviors are effective as inappropriate clustering in risk-prone locations may instead increase urban flood risk. To investigate mobility-induced urban flood risk exposure changes, we extracted a flood map in Jiangsu over the research time window from Google Maps^{S4} where inundated urban areas are labeled at a resolution of 30 m. We then overlaid the flood map, population map, and city boundary map on the “mobility map” and calculated an index to reflect the changes in urban flood risk exposure, as shown in eq 4

$$\Delta \text{floodRisk}_i = \frac{\sum_{k \in G_i} \text{visit}_{\text{shock}(k)} \times \text{POP}_k \times \text{flood}_k}{\sum_{k \in G_i} \text{POP}_k \times \text{visit}_{\text{shock}(k)}} \times 100\% \quad (4)$$

where $\Delta \text{FloodRisk}_i$ is the change of urban flood risk exposure in city i , as measured by percentage changes in population within urban floodplains due to mobility; G_i denotes all the flood grids in city i ; $\text{visit}_{\text{shock}(k)}$ is the change of human mobility in grid k ; and POP_k indicates the population in grid k . flood_k is a binary variable and is coded with 1 if grid k is inundated and with 0 if not.

4. RESULTS AND DISCUSSION

4.1. Human Mobility Changes in Response to Rainfall Events. As visualized in Figure 2(A), the $\text{visit}_{\text{shock}}$ indicator, measuring percent changes in human activities at the 500 m × 500 m grid cell level, well represents urban residents’ responses

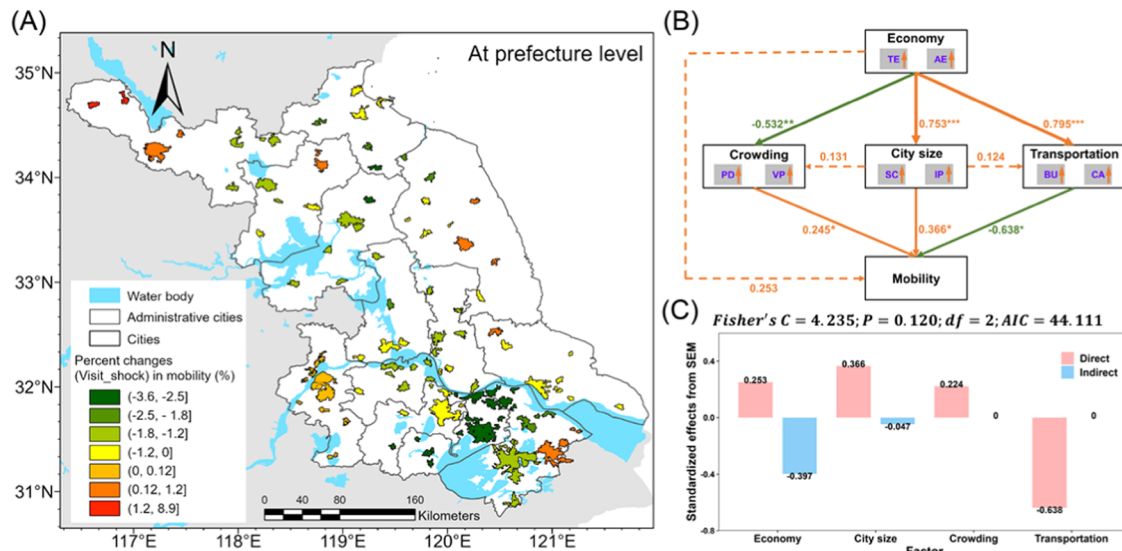


Figure 3. Changes in human mobility after heavy rainfall at the prefecture level and potential drivers. (A) Percent changes in mobility at the prefecture level. (B) Results of piecewise SEM between changes in mobility and eight explanatory variables. Colors are used to distinguish the direction of correlation (orange for positive correlation and green for negative correlation) (* $p < 0.05$; ** $p < 0.01$; *** $p < 0.001$). (C) Direct and indirect effects of the four latent variables.

to rainfall events. There are about 0.16 million grids in Jiangsu Province (excluding large water bodies), and more than a third of them (~54 thousand grids) capture changes in human mobility after precipitation. The distribution of affected grids is more centered in the urban area than the rural region probably due to intensive social activities and dense road networks in cities.

The directions of the changes in human mobility are also mixed. For example, zooming in on the maps of two urban agglomeration areas, Nanjing and Suzhou (Figure 2B,C), we find places affected by rainfalls are clustered and intertwined but show different spatial patterns across cities. In Nanjing, there is an increasing trend of human activities (red squares) in the urban center but a decreasing trend in suburbs (blue squares). While in Suzhou, the pattern is different with overall attenuated human activities in the downtown area. This may be due to the proximity of the two cities to two different types of large bodies of water with different proximities. To identify hotspots of spatial clusters with similar patterns of human mobility changes, we further conducted Anselin Local Moran's I analysis⁵⁵ for the whole province Figure S5. This map is favorable for the detection of large volumes of people flow within the cities and efficient emergency resource allocation.

We find grid-level absolute changes in human mobility after heavy rainfall events range between 0 and 87.4%, having a mean value of 3.2%. When drawing density plots to examine grid-level mobility changes between urban and rural areas (see Figure S6) that distinguished according to the functional urban boundary proposed by Ma and Long,⁵⁰ we find that data distributions are both left-skewed with more than 80% of grids having a change in mobility less than 5%. However, grids in the urban area with absolute mobility change greater than 15% are about 20% more than those in rural regions. We perform *t* test and demonstrate significant differences in grid-level mobility changes between urban and rural areas ($t = 12.102$, $p < 0.001$), indicating that residents' activities in cities tend to be more easily affected by heavy rainfall events.

4.2. Potential Drivers of Human Mobility Changes at the Prefecture Level.

We aggregate grid-level human

mobility changes to the prefecture level according to the cities' boundaries Figure 3(A). The grid-level population is chosen as the weight when aggregating the data. We find that prefecture-level changes in mobility vary ranging from -3.6 to 8.9% (excluding two counties, Feng and Pei, over 8%, the range becomes -3.6–1.2%). It indicates that the mobility changes within cities are not balanced. Some cities have shown increased aggregated mobility, which may indicate more crowded conditions after rainfall shocks, while some others have shown decreased aggregated mobility, which may indicate overall reduced human activities to avoid risks.

To explain heterogeneity across cities in the mobility pattern, we applied piecewise SEM to reveal indirect and spurious relationships between aggregated mobility change and four prefecture-level latent variables (as shown in Figure 3(B)). We first examine the direct impacts of four latent variables on changes in population mobility. The latent variable "transportation" displays a significant negative correlation with mobility change, indicating that cities with more robust transportation systems reduce the likelihood of abnormal population clustering during rainfall, as shown by decreased aggregated mobility ($\beta = -0.638$, $p = 0.032$). The latent variable "crowding" is positively correlated with mobility change, suggesting that a high density of elder people with limited mobility predicts a greater degree of abnormal population clustering ($\beta = 0.245$, $p = 0.048$). Moreover, the latent variable "city size" plays a role in increasing mobility after rainfalls, indicating that large cities are more likely to have population clustering ($\beta = 0.366$, $p = 0.041$). Lastly, the latent variable "economy" does not directly influence mobility ($\beta = 0.253$, $p = 0.398$).

We then examine all potential relationships between variables and identify three indirect pathways that a city's economic condition may affect residents' mobility responses to heavy rainfalls. First, "Economy" positively influences "transport" ($\beta = 0.795$, $p = 0.000$) and supports the reduction of mobility. It indicates that developed cities facilitate people to evacuate and avoid clustering after rainfall with better-designed public transportation systems. Second, "economy" negatively

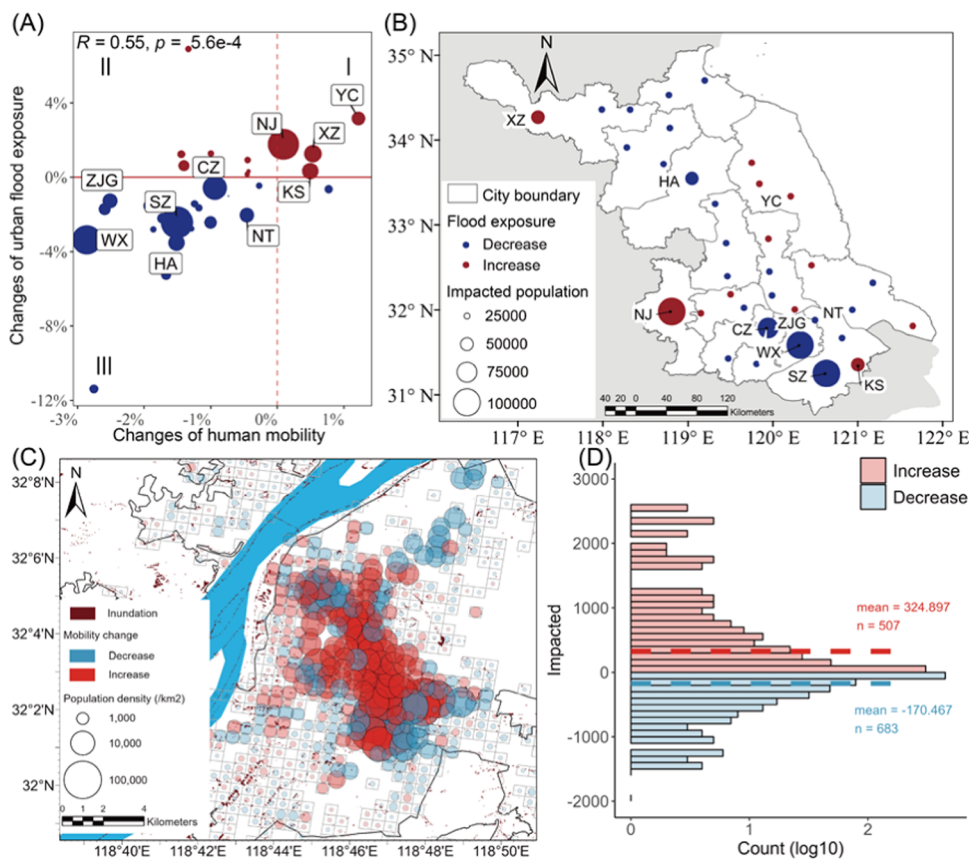


Figure 4. Change in urban flood risk exposure per city and its association with human mobility after heavy rainfalls. (A, B) Changes in flood risk exposure after heavy rainfalls. The size of the point is proportional to the change in the number of people staying in areas at risk of flooding. The color of the point indicates the direction of change. (C) Process of overlaying four layers. (D) Histogram of the impacted population in the flood-prone grid.

correlates with “crowding” ($\hat{\beta} = -0.532, p = 0.008$) and indirectly reduces mobility after heavy precipitation, as shown in Figure 3(C). It might be because developed cities are associated with more urban spaces and young age citizens, which reduces the likelihood of people crowding. Third, “economy” is associated with expanded “city size,” which, in turn, induces higher aggregated mobility ($\hat{\beta} = 0.753, p = 0.000$). It indicates that megacities with not only developed economies but also large urban sizes and populations are more likely to face abnormal crowding after heavy rain shocks. Detailed information about the model can be seen in Tables S4–S6.

4.3. Mobility Changes Reveal Urban Flood Risk Maladaptation. When heavy rainfall occurs, people may adopt adaptation behaviors such as seeking shelters, which will increase or decrease the time people stay in a certain place and reshape the patterns of urban flood risk exposure. We thus overlay inundation hotspot maps on grid-level mobility change maps to calculate prefecture-level flood risk exposure changes. Figure 4 presents how the changes in urban flood risk exposures are associated with aggregated human mobility dynamics after rainfall events.

We found a significant positive correlation between population mobility and urban flood risk exposure ($\hat{\beta} = 1.50, p = 5.6e-4$). This suggests that given the current urban development status of each city in Jiangsu Province, reducing population mobility during rainfall periods can be beneficial for urban flood risk adaptation. Moreover, Figure 4(A) reflects the

flood risk adaptation status of different cities in Jiangsu. As presented by blue circles in Quadrant III, urban residents’ activities and flood exposure both decreased in 23 cities as the result of sudden precipitation shocks. A mean of 2.6% urban flood risk can be avoided in this group, with a total affected population of 0.45 million. Cities where risk-reduction effects are prominent include Suzhou (SZ), Wuxi (WX), and Changzhou (CZ). On the opposite, five cities including Nanjing city (NJ) have a mean of 1.4% increase in flood risk exposure with a total affected population of 0.18 million, as shown by red circles in Quadrant I. We also notice that seven cities fallen in Quadrant II are those having declined human activities but rising urban flood risk exposure. Human mobility instead increases the exposure to flood risks in these two types of cities, thereby raising the risk level of the cities, suggesting that these cities are experiencing flood risk maladaptation.

To validate our findings, we employ Nanjing as a case study, specifically examining population mobility within urban flood-prone areas at a 500 m grid scale during rainfall events. The results are presented in Figure 4(C), where the circle size represents the grid’s population, and color signifies changes in mobility during rainfall. Notably, during rainfall, population mobility in Nanjing shifted toward central areas, indicating a net influx into high-risk zones. Figure 4(D) further reinforces these observations. In this figure, we calculated changes in population mobility in flood-prone grid areas by considering the population, resulting in a frequency distribution histogram. The results reveal that 683 areas experienced a population

decrease (average -170.467), while 507 areas witnessed an increase in population (average 324.897), indicating that flood-prone regions exhibited a net population increase.

4.4. Implications for Urban Flood Risk Management.

Our study provides valuable implications for urban flood risk management from two aspects. First, our research offers a framework to map the hotspots of human mobility and urban flood risk after heavy precipitation by integrating real-time mobile phone signaling big data. This is helpful to enhance the early warning system of urban flooding by tracing where citizens are moving toward and identifying clusters with higher inundation risks. The map is also useful to inform citizens in advance about areas where flooding is likely to occur so that they can optimize travel decision-making. This alerting system is especially urgent to reduce the population flow that moves to risky areas due to limited information, which is urgently needed in those cities exhibiting maladaptation toward flood risks (Figure 4). In addition, the map can also guide residents in risky areas to evacuate in advance when rainfall occurs to prevent secondary disasters caused by human mobility dynamics.

The second implication is that we have revealed factors that drive the urban vulnerability toward heavy rainfalls, which is informative for the long-term capacity building of urban climate adaptation. As shown in the piecewise SEM model, we find that basic infrastructure such as a public transportation network, economic situation, and vulnerability of the population can significantly influence the magnitude and direction of human mobility. Accordingly, better management of urban transportation networks is one of the most efficient approaches to cope with mobility-induced urban flood risks in the context of climate change. Compared to other socio-economic sectors, commercial activities are more vulnerable in the face of the shocks of extreme weather events. The findings suggest urban decision-makers increase local economic diversity and develop innovative markets to enhance flood risk adaptation.

Our work also sheds light on theoretical insights into studies of urban flood risk at a high spatial and temporal resolution. Using 2.6 million mobile phone signal data to quantify human mobility, the method bridges the knowledge gap between heavy rainfall, individual adaptation strategies, and urban flood risk. The results reveal that human mobility changes exhibit different patterns not only between cities but also within cities. Previous studies that examined human mobility response to weather events have mainly focused on extremely adverse natural disasters such as typhoons or earthquakes.²⁰ They generally have coarse spatial resolution and focus on migration behaviors before and after the disasters. This study extends current frameworks so that we can monitor public mobility changes when high-frequency and moderate-heavy rainfall events occur. Taking advantage of the high-resolution mobility and urban flood maps, we also reveal that poor city management may lead to maladaptation so that more residents are exposed to flood risks as they change their trip modes.

Several limitations in our study should be acknowledged here. First, our data were obtained from Jiangsu Telecom, whose subscribers account for roughly 35% of the total population in Jiangsu Province. Although our analysis (Figure S2) shows that mobile phone signaling data have a good representation of the local population and human mobility patterns at scale, there might exist differences across cities due to the varied proportion of subscribers. Meanwhile, our mobile

phone data were obtained from 5 years ago. More recent data may enable us to carry out research on a finer spatial and temporal scale due to more advanced position-tracking technologies. Second, although we have applied algorithms to attempt to remove trend effects such as short-term weekly fluctuations and long-term user increases, it is difficult to control all the confounding factors that affect the patterns of mobile phone signals, e.g., traffic accidents, construction projects, and other important public events. Unlike us, in the work of Metulini et al.,⁵⁶ they decomposed mobile phone signaling data in days and focused on seasonal structure, which is also an amazing attempt. In the future, it will be worthwhile to compare the robustness of these two approaches. Third, given data availability, our study does not track any specific users, and it is not possible to depict user-level intracity trip decision-makings or to capture intercity population movement. The urban flood maps we use were also based on historical records and do not reflect instant inundation hotspots. It is expected that incorporating more refined human-centric data (e.g., contents on social media) in the future could help us gain more understanding of how the impacts of small-scale natural hazards vary among people with different backgrounds.⁵⁷ At the same time, our study reveals the potential impact of different water body types and distances from water bodies on population movement, and we believe that it would be worthwhile to incorporate such spatial effects into the model.

ASSOCIATED CONTENT

Supporting Information

The Supporting Information is available free of charge at <https://pubs.acs.org/doi/10.1021/acs.est.3c03145>.

Introduction to S-H-ESD method; general and geographic information about 53 cities and mobile phone towers in Jiangsu, China; examples of mobile phone signaling data; data validation including rainfall data and mobile phone signaling data; comparison and validation of baseline calculation method; analyses results related to piecewise SEM; explanatory variables data source; Anselin Local Moran's I analysis of mobility changes; and differences in mobility changes between rural and urban areas ([PDF](#))

AUTHOR INFORMATION

Corresponding Authors

Jianxun Yang — State Key Laboratory of Pollution Control and Resource Reuse, School of the Environment, Nanjing University, Nanjing 210023, China; Jiangsu Collaborative Innovation Center of Atmospheric Environment and Equipment Technology (CICAET), Nanjing University of Information Science & Technology, Nanjing 210044 Jiangsu, China; orcid.org/0009-0005-0821-7698; Email: yangjx@nju.edu.cn

Miaomiao Liu — State Key Laboratory of Pollution Control and Resource Reuse, School of the Environment, Nanjing University, Nanjing 210023, China; Jiangsu Collaborative Innovation Center of Atmospheric Environment and Equipment Technology (CICAET), Nanjing University of Information Science & Technology, Nanjing 210044 Jiangsu, China; orcid.org/0000-0002-9043-3584; Email: liumm@nju.edu.cn

Authors

- Jiacong Cai — State Key Laboratory of Pollution Control and Resource Reuse, School of the Environment, Nanjing University, Nanjing 210023, China
- Wen Fang — State Key Laboratory of Pollution Control and Resource Reuse, School of the Environment, Nanjing University, Nanjing 210023, China;  orcid.org/0000-0001-5669-322X
- Zongwei Ma — State Key Laboratory of Pollution Control and Resource Reuse, School of the Environment, Nanjing University, Nanjing 210023, China
- Jun Bi — State Key Laboratory of Pollution Control and Resource Reuse, School of the Environment, Nanjing University, Nanjing 210023, China; Jiangsu Collaborative Innovation Center of Atmospheric Environment and Equipment Technology (CICAET), Nanjing University of Information Science & Technology, Nanjing 210044 Jiangsu, China

Complete contact information is available at:
<https://pubs.acs.org/10.1021/acs.est.3c03145>

Notes

The authors declare no competing financial interest.

ACKNOWLEDGMENTS

The project was financially supported by the National Natural Science Foundation of China (Grant Nos 72304136, 72222012, 71921003, and 52170189), National Postdoctoral Program for Innovative Talent (Grant No. BX20230159), Jiangsu R&D Special Fund for Carbon Peaking and Carbon Neutrality (Grant No. BK20220014), and Jiangsu Natural Science Foundation (Grant No. BK20220125). Dr. Jianxun Yang acknowledges the Yuxiu Young Scholar Postdoc Fellowship granted by Nanjing University and the Research Committee of the School of Environment, Nanjing University, for approving this study.

REFERENCES

- (1) Pörtner, H.-O.; Roberts, D. C.; Adams, H.; Adler, C.; Aldunce, P.; Ali, E.; Begum, R. A.; Betts, R.; Kerr, R. B.; Biesbroek, R. *Climate Change: Impacts, Adaptation, and Vulnerability* 2022; IPCC Sixth Assessment Report, 2022.
- (2) Harrison, C. G.; Williams, P. R. A systems approach to natural disaster resilience. *Simul. Modell. Pract. Theory* **2016**, *65*, 11–31. (accesced 2022-10-23)
- (3) Huang, Y.; Tian, Z.; Ke, Q.; Liu, J.; Irandehzad, M.; Fan, D.; Hou, M.; Sun, L. Nature-based solutions for urban pluvial flood risk management. *Wiley Interdiscip. Rev.: Water* **2020**, *7* (3), No. e1421.
- (4) Hammond, M. J.; Chen, A. S.; Djordjević, S.; Butler, D.; Mark, O. Urban flood impact assessment: A state-of-the-art review. *Urban Water J.* **2015**, *12* (1), 14–29.
- (5) Winsemius, H. C.; Aerts, J. C.; Van Beek, L. P.; Bierkens, M. F.; Bouwman, A.; Jongman, B.; Kwadijk, J. C.; Ligtoet, W.; Lucas, P. L.; Van Vuuren, D. P.; Ward, P. J. Global drivers of future river flood risk. *Nat. Clim. Change* **2016**, *6* (4), 381–385.
- (6) Rentschler, J.; Salhab, M.; Jafino, B. A. Flood exposure and poverty in 188 countries. *Nat. Commun.* **2022**, *13* (1), No. 3527.
- (7) Alexander, L. V.; Zhang, X.; Peterson, T. C.; Caesar, J.; Gleason, B.; Klein Tank, A.; Haylock, M.; Collins, D.; Trewin, B.; Rahimzadeh, F. et al. Global observed changes in daily climate extremes of temperature and precipitation. *J. Geophys. Res.: Atmos.* **2006**; Vol. 111 D5 DOI: [10.1029/2005JD006290](https://doi.org/10.1029/2005JD006290).
- (8) Rus, K.; Kilar, V.; Koren, D. Resilience assessment of complex urban systems to natural disasters: A new literature review. *Int. J. Disaster Risk Reduct.* **2018**, *31*, 311–330.
- (9) Kuzma, S.; Luo, T. *The Number of People Affected by Floods Will Double between 2010 and 2030*; World Resources Institute, 2020. (accessed 2022-10-23).
- (10) Assembly, U. G.. Transforming our world: the 2030 agenda for sustainable development, 21 October 2015 2015. Retrieved from.
- (11) Pradhan, P.; Costa, L.; Rybski, D.; Lucht, W.; Kropp, J. P. A systematic study of sustainable development goal (SDG) interactions. *Earth's Future* **2017**, *5* (11), 1169–1179.
- (12) Mansour, M. M.; Ibrahim, M. G.; Fujii, M.; Nasr, M. Sustainable development goals (SDGs) associated with flash flood hazard mapping and management measures through morphometric evaluation. *Geocarto Int.* **2022**, *37* (26), 11116–11133.
- (13) Sebestyén, V.; Dörgö, G.; Ipkovich, Á.; Abonyi, J. Identifying the links among urban climate hazards, mitigation and adaptation actions and sustainability for future resilient cities. *Urban Climate* **2023**, *49*, No. 101557.
- (14) Pour, S. H.; Abd Wahab, A. K.; Shahid, S.; Asaduzzaman, M.; Dewan, A. Low impact development techniques to mitigate the impacts of climate-change-induced urban floods: Current trends, issues and challenges. *Sustainable Cities Soc.* **2020**, *62*, No. 102373.
- (15) Sanders, B. F.; Schubert, J. E.; Goodrich, K. A.; Houston, D.; Feldman, D. L.; Basolo, V.; Luke, A.; Boudreau, D.; Karlin, B.; Cheung, W.; et al. Collaborative modeling with fine-resolution data enhances flood awareness, minimizes differences in flood perception, and produces actionable flood maps. *Earth's Future* **2020**, *8* (1), No. e2019EF001391.
- (16) Leis, J.-L.; Kienberger, S. Climate risk and vulnerability assessment of floods in Austria: Mapping homogenous regions, hotspots and typologies. *Sustainability* **2020**, *12* (16), 6458.
- (17) Winsemius, H. C.; Van Beek, L.; Jongman, B.; Ward, P.; Bouwman, A. A framework for global river flood risk assessments. *Hydrol. Earth Syst. Sci.* **2013**, *17* (5), 1871–1892.
- (18) De Moel, H.; Jongman, B.; Kreibich, H.; Merz, B.; Penning-Roselli, E.; Ward, P. J. Flood risk assessments at different spatial scales. *Mitigation Adaptat. Strategies Global Change* **2015**, *20*, 865–890.
- (19) Cariolet, J.-M.; Vuillet, M.; Diab, Y. Mapping urban resilience to disasters—A review. *Sustainable Cities Soc.* **2019**, *51*, No. 101746.
- (20) Wang, Q.; Taylor, J. E. Patterns and limitations of urban human mobility resilience under the influence of multiple types of natural disaster. *PLoS One* **2016**, *11* (1), No. e0147299.
- (21) Roy, K. C.; Cebrian, M.; Hasan, S. Quantifying human mobility resilience to extreme events using geo-located social media data. *EPJ Data Sci.* **2019**, *8* (1), 18.
- (22) Kang, C.; Ma, X.; Tong, D.; Liu, Y. Intra-urban human mobility patterns: An urban morphology perspective. *Phys. A* **2012**, *391* (4), 1702–1717.
- (23) Rahimi-Golkhandan, A.; Garvin, M. J.; Wang, Q. Assessing the impact of transportation diversity on postdisaster intraurban mobility. *J. Manage. Eng.* **2021**, *37* (1), No. 04020106.
- (24) Pan, X.; Han, C. S.; Dauber, K.; Law, K. H. A multi-agent based framework for the simulation of human and social behaviors during emergency evacuations. *Ai Soc.* **2007**, *22* (2), 113–132.
- (25) Cutter, S. L.; Burton, C. G.; Emrich, C. T. Disaster resilience indicators for benchmarking baseline conditions. *J. Homeland Secur. Emerg. Manage.* **2010**; Vol. 7 DOI: [10.2202/1547-7355.1732](https://doi.org/10.2202/1547-7355.1732).
- (26) Cutter, S. L.; Ash, K. D.; Emrich, C. T. The geographies of community disaster resilience. *Global Environ. Change* **2014**, *29*, 65–77.
- (27) Ahas, R.; Silm, S.; Saluveer, E.; Järv, O. Modelling Home and Work Locations of Populations Using Passive Mobile Positioning Data. In *Location based Services and TeleCartography II*; Springer, 2009; pp 301–315.
- (28) Jiang, S.; Ferreira, J.; Gonzalez, M. C. Activity-based human mobility patterns inferred from mobile phone data: A case study of Singapore. *IEEE Trans. Big Data* **2017**, *3* (2), 208–219.
- (29) González, M. C.; Hidalgo, C. A.; Barabási, A.-L. Understanding individual human mobility patterns. *Nature* **2008**, *453* (7196), 779–782.

- (30) Eyre, R.; De Luca, F.; Simini, F. Social media usage reveals recovery of small businesses after natural hazard events. *Nat. Commun.* **2020**, *11* (1), No. 1629.
- (31) Kryvasheyeu, Y.; Chen, H.; Obradovich, N.; Moro, E.; Hentenryck, P. V.; Fowler, J.; Cebrian, M. Rapid assessment of disaster damage using social media activity. *Sci. Adv.* **2016**, *2* (3), No. e1500779.
- (32) Qian, J.; Du, Y.; Yi, J.; Liang, F.; Wang, N.; Ma, T.; Pei, T. Quantifying unequal urban resilience to rains across China from location-aware big data. *Nat. Hazards Earth Syst. Sci. Discuss.* **2022**, *1*–20.
- (33) Rajput, A. A.; Mostafavi, A. Latent Sub-structural Resilience Mechanisms in Temporal Human Mobility Networks during Urban Flooding. *Sci. Rep.* **2023**, *13* (1), 10953.
- (34) Cao, J.; Li, Q.; Tu, W.; Gao, Q.; Cao, R.; Zhong, C. Resolving urban mobility networks from individual travel graphs using massive-scale mobile phone tracking data. *Cities* **2021**, *110*, No. 103077.
- (35) Song, C.; Qu, Z.; Blumm, N.; Barabási, A.-L. Limits of predictability in human mobility. *Science* **2010**, *327* (5968), 1018–1021.
- (36) Lu, X.; Wetter, E.; Bharti, N.; Tatem, A. J.; Bengtsson, L. Approaching the limit of predictability in human mobility. *Sci. Rep.* **2013**, *3* (1), No. 2923.
- (37) Perazzini, S.; Metulini, R.; Carpita, M. Statistical indicators based on mobile phone and street maps data for risk management in small urban areas. *Stat. Methods Appl.* **2023**, *1*–28.
- (38) Lai, S.; Ruktanonchai, N. W.; Zhou, L.; Prosper, O.; Luo, W.; Floyd, J. R.; Wesolowski, A.; Santillana, M.; Zhang, C.; Du, X.; et al. Effect of non-pharmaceutical interventions to contain COVID-19 in China. *Nature* **2020**, *585* (7825), 410–413.
- (39) Lu, X.; Bengtsson, L.; Holme, P. Predictability of population displacement after the 2010 Haiti earthquake. *Proc. Natl. Acad. Sci. U.S.A.* **2012**, *109* (29), 11576–11581.
- (40) Blanford, J. I.; Huang, Z.; Saveliev, A.; MacEachren, A. M. Geo-located tweets. Enhancing mobility maps and capturing cross-border movement. *PLoS One* **2015**, *10* (6), No. e0129202.
- (41) González, M. C.; Hidalgo, C. A.; Barabasi, A.-L. Understanding individual human mobility patterns. *Nature* **2008**, *453* (7196), 779–782.
- (42) Buckee, C.; Noor, A.; Sattenspiel, L. Thinking clearly about social aspects of infectious disease transmission. *Nature* **2021**, *595* (7866), 205–213.
- (43) Mu, X.; Huang, A.; Wu, Y.; Xu, Q.; Zheng, Y.; Lin, H.; Fang, D.; Zhang, X.; Tang, Y.; Cai, S. Characteristics of the precipitation diurnal variation and underlying mechanisms over Jiangsu, eastern China, during warm season. *Front. Earth Sci.* **2021**, *9*, No. 703071.
- (44) Zhou, Q.; Qu, S.; Ding, J.; Liu, M.; Huang, X.; Bi, J.; Ji, J. S.; Kinney, P. L. Association between PM2.5 and daily pharmacy visit tendency in China: A time series analysis using mobile phone cellular signaling data. *J. Cleaner Prod.* **2022**, *340*, No. 130688.
- (45) Xin, X.; Wu, T.; Zhang, J.; Yao, J.; Fang, Y. Comparison of CMIP6 and CMIP5 simulations of precipitation in China and the East Asian summer monsoon. *Int. J. Climatol.* **2020**, *40* (15), 6423–6440.
- (46) Vallis, O.; Hochenbaum, J.; Kejariwal, A. A Novel Technique for Long-Term Anomaly Detection in the Cloud. In *6th USENIX Workshop on Hot Topics in Cloud Computing (HotCloud 14)* 2014.
- (47) Hersbach, H.; Bell, B.; Berrisford, P.; Biavati, G.; Horányi, A.; Muñoz Sabater, J.; Nicolas, J.; Peubey, C.; Radu, R.; Rozum, I. ERA5 hly Data on Single Levels from 1979 to Present *Copernicus Climate Change Service (C3S) Climate Data Store (CDS)* 2018; Vol. 10.
- (48) Ye, H.; China Meteorological News Agency. Rainfall Rating 2018 https://www.cma.gov.cn/2011xzt/2018zt/20100728/2010072804/201807/t20180706_472586.html. accessed Oct 23, 2022.
- (49) Dujardin, S.; Jacques, D.; Steele, J.; Linard, C. Mobile phone data for urban climate change adaptation: Reviewing applications, opportunities and key challenges. *Sustainability* **2020**, *12* (4), 1501.
- (50) Ma, S.; Long, Y. Identifying spatial cities in China at the community scale. *J. Urban Reg. Plan* **2019**, *11*, 37–50.
- (51) Shipley, B. Confirmatory path analysis in a generalized multilevel context. *Ecology* **2009**, *90* (2), 363–368.
- (52) Shipley, B. A new inferential test for path models based on directed acyclic graphs. *Struct. Equation Model.* **2000**, *7* (2), 206–218.
- (53) Johnson, C.; Blackburn, S. Advocacy for urban resilience: UNISDR's making cities resilient campaign. *Environ. Urbanization* **2014**, *26* (1), 29–52.
- (54) Mehmood, H.; Conway, C.; Perera, D. Mapping of Flood Areas Using Landsat with Google Earth Engine Cloud Platform. *Atmosphere* **2021**, *12* (7), 866.
- (55) Anselin, L. Local indicators of spatial association—LISA. *Geogr. Anal.* **1995**, *27* (2), 93–115.
- (56) Metulini, R.; Carpita, M. Modeling and forecasting traffic flows with mobile phone big data in flooding risk areas to support a data-driven decision making. *Ann. Oper. Res.* **2023**, *1*–26.
- (57) Wang, B.; Loo, B. P.; Zhen, F.; Xi, G. Urban resilience from the lens of social media data: Responses to urban flooding in Nanjing, China. *Cities* **2020**, *106*, No. 102884.